Analysis of High-Index Contrast Lithium Niobate Waveguides Fabricated by High Vacuum Proton Exchange

Alicia Petronela Rambu, Alin Marian Apetrei, Florent Doutre, Hervé Tronche, Marc de Micheli, Sorin Tascu

Analysis of High-Index Contrast Lithium Niobate Waveguides Fabricated by High Vacuum Proton Exchange

Alicia Petronela Rambu[1], Alin Marian Apetrei[1], Florent Doutre[2], Hervé Tronche[2], Marc de Micheli[2] and Sorin Tascu[1]

1 : Research Center on Advanced Materials and Technologies, Sciences Department, Alexandru Ioan Cuza University of Iasi, Blvd. Carol I, no. 11, 700506 Iasi, Romania

2 : Institut de Physique de Nice, UMR 7010, Université Côte d'Azur, CNRS, Avenue Joseph Vallot, Parc Valrose, 06100 Nice, France

Abstract—High-index contrast waveguides fabricated with precise control and reproducibility are of high interest for nonlinear and/or electro-optical highly efficient and compact devices for quantum and classical optical data processing. Here we present a new process to fabricate planar and channel optical waveguides on lithium niobate substrates that we called High Vacuum Proton Exchange (HiVacPE). The main purpose was to improve the reproducibility and the quality of the produced waveguides by limiting and controlling the water traces in the melt, which is used for the ionic exchange. Moreover, we discovered that, when the acidity of the bath is increased, depending on substrate orientation (Z-cut or X-cut) the waveguides are completely different in term of crystallographic properties, index profiles and nonlinearity. The best-obtained channel waveguides exhibit a refractive index contrast as high as 0.04 without any degradation of the crystal nonlinearity and state of the art propagation losses (0.16dB/cm). We have also demonstrated that the HiVacPE process allows fabricating waveguides on Z-cut substrate with high-index contrast up to 0.11 without degrading the crystal nonlinearity but high strain induced propagation losses. On top of that, we proposed an original and very useful method of analyzing waveguides with complex index profiles. This method can be used for the analysis of any waveguides whose core contains several layers.

Index Terms—lithium niobate, nonlinear optics, optical waveguides.

I. Introduction

Lithium Niobate (LN) crystal of high optical quality and wide transparency range (350-5200 nm) is already one of the most used materials for many integrated optical applications and photonic devices. Its excellent electro-optical and nonlinear optical properties are exploited in various applications such as: laser frequency doublers, wideband tunable light sources, light amplification, quasi-phase-matched frequency convertors, surface acoustic waves, optical switches and modulators, multiplexors and for many other all-optical signals processing. Most of the integrated optics devices designed for these applications are based on waveguides fabricated either by Ti-indiffusion [1, 2] or by one of the proton exchange techniques namely Annealed Proton Exchange (APE) [3-5], Reverse Proton Exchange (RPE) [6] or Soft Proton Exchange (SPE) [7-10]. All these techniques allow fabricating low loss waveguides with preserved electro- optical and nonlinear properties, but in return lead to low refractive index increase typically in the range of Δn_e=0.01 for Ti-indiffusion [11], Δn_e=0.02 for APE and RPE [6] and Δn_e=0.03 for SPE [7]. These values limit the benefit linked to the confinement of the lights in a waveguide. The maximum index contrast allowed by the Proton Exchange (PE) technique [12] is approximately Δn_e=0.12 at λ=633 nm but most of waveguides exhibiting such a Δn_e present a nonlinear coefficient $\chi^{(2)}$ totally degraded [13]. Recently, the so-called High Index Soft Proton Exchange (HISoPE) allowed the fabrication of channel waveguides that exhibit Δn_e=0.1 with almost unmodified nonlinearities but high strain induced propagation losses (≥5dB/cm) [14].

In this paper, we propose to focus on the influence of the high vacuum and water traces in the exchange ampoule on the quality of the waveguides obtained in fabrication conditions that are near the transition PE-SPE (high Δn_e /low Δn_e).

Proposed at the beginning of the 80's [12], the Proton Exchange (PE) technique is a chemical fabrication process of waveguides and consists in immersing a LN sample in an acidic bath at temperature ranging from 200°C to 400°C. Most of the time, the acidic bath consists in melted benzoic acid, but despite its low acidity one can also use pure water or water vapor [15-18]. It is therefore important to consider the influence of water traces in acidic melts as they can modify the acidity of the bath through self-ionization or modification of the acid ionization [19]. This is a key feature to control, as the acidity has a strong impact on the refractive index contrast, the crystallographic structure, the nonlinearity and the propagation losses of the final waveguides [20]. It has also to be controlled to obtain reproducible results.
Here we study a new fabrication technique that we named High Vacuum Proton Exchange (HiVacPE) which consists in pumping harder the exchange ampoule to diminish as much as possible the water content of the acidic bath. Beside expected effects such as the modification of the position of the PE-SPE transition threshold, we observed strong differences between the HiVacPE waveguides prepared on X-cut and Z-cut substrate, which have never been reported so far. On top of these important results for the fabrication of integrated optics circuits, we will also describe an original and very useful method for the analysis of waveguides whose core contains several layers.

II. HIGH VACUUM PROTON EXCHANGE (HIVACPE)

High Vacuum Proton Exchange process was performed in a hermetically sealed hourglass tube. Prior to be sealed, the bottom part of the tube was filled with a powder mixture composed of Benzoic Acid (BA) and Lithium Benzoate (LB) as proton source. The concentration of LB in the melt is measured by $\varrho_{LB}=100\times[m_{LB}/(m_{LB}+m_{BA})]$ where m_{LB}, and m_{BA} are the mass of LB and BA in the powder mixture. The sample to be processed is placed in the top part of the tube and then, by using a turbo pumping station (HiCube 80 Eco - Pfeiffer), the tube is pumped down to a pressure as low as $p=3.5\times10^{-5}$ mbar. This very low pressure, 10^5 times lower compared to the ones reported by the literature [14, 21], is the key point of the HiVacPE technique which allows diminishing as much as possible the residual water adsorbed by the internal surface of the glass tube and mainly the large amount absorbed by powders. After the glass tube is sealed, it is placed into a metallic tube container ensuring a uniform heating and an easy and safe manipulation. Placed in an oven, that was prior heated at 300 °C, the metallic tube is turned upside down after 30 minutes when both the melted proton source and the sample have reached the exchange temperature. Thus, the sample is dipped into the melt and the proton exchange starts. At the end of the exchange period (t=72 hours), the tube is turned upside down again and allowed to cool down. When it reaches the room temperature, breaking the sealed-end allows getting out the sample. Using this protocol, we fabricated planar HiVacPE waveguides on both Z-cut and X-cut LN samples. The samples were cut from wafers supplied by Gooch & Housego. The BA and LB powders supplied by Sigma-Aldrich were mixed in concentrations of LB ranging from 3% down to 2.2% with an increment of 0.1%.
In this range of LB content, one finds the threshold ϱ_{th}, which is the minimum LB amount necessary to obtain low- index contrast SPE waveguides at 300°C. For lower LB amount, one obtains the high-index contrast waveguides [14, 21]. This threshold marks an important change in both the crystallographic structure and the index profile of the waveguides. From the crystallographic point of view, one goes from a single layer waveguide where only the α-phase is present, to a multi-layer structure where both $\varkappa$ phases and α- phase are present in the protonated area. From the index profile point of view, one goes from an exponential index profile for SPE waveguides to the mix of a step and a gradient profile in high index waveguides [14].
The main purpose when started working on HiVacPE was to improve the reproducibility and the quality of the fabricated waveguides by limiting and controlling the water traces in the melt. The impact of HiVacPE process on the reproducibility was tested over one year and a half by producing, in same vacuum conditions, more than fifty waveguides by using different LB concentrations in the range of 3% and 2.2%. For laboratory experiments and demonstrators both, planar and channel waveguides have been fabricated and no notable differences were identified in index profile behavior, index contrast, nonlinearity and propagation losses. We can say that HiVacPE is a trouble-free and highly reproducible process allowing producing efficient and compact devices for applications in modern photonics.

III. HiVacPE PLANAR WAVEGUIDES

A. Crystallographic investigation by X-Ray Diffraction

To investigate the crystalline structure and the modification of lattice parameters of HiVacPE planar waveguides, we used the X-ray diffraction method (XRD). We chose to use the rocking curves of crystallographic planes parallel to the surface of Z- cut and X-cut of LN samples with Miller indices: h=0, k=0, l=12 (00.12) for Z-cut and h=2, k=2, l=0 (220) for X-cut corresponding respectively to $\theta_{B,Z\text{-}cut}$=41.8062° and $\theta_{B,X\text{-}cut}$=73.479° Bragg angles in the substrate. These values are used as origin in the spectra reported on Fig. 1. It is worth to note that the lattice parameters of the proton exchanged layer are greater than those of the substrate [22]. In the case of a planar waveguide and considering the stress induced by the non-protonated substrate, the only allowed deformations are normal to the surface of the sample [23]. The strain ε_{33}" perpendicular to the surface can be obtained directly from the rocking curves. It is expressed as:

$$\varepsilon"_{33} = -\Delta\theta_{hkl} \cdot \cot\theta_B \qquad (1)$$

where $\Delta\theta_{hkl}$ is the measured angular distance between the substrate peak and protonated layer peak on the rocking curve from the surface plane (hkl), in our case (00.12) and (220) respectively. It was demonstrated that the surface layer always presents the largest value of the strain [23]. Starting from the rocking curves we identify the crystallographic phases and also calculate the value of the strain by using (1) and compare them to those reported in literature [23, 24].

The HiVacPE waveguides present interesting crystallographic structures and exhibit characteristics that are worth to be noted.

In the case of Z-cut samples, Fig. 1(a), for ϱ_{LB} ranging from 3% to 2.5% only α-phase is identified, the maximum intensity peak of this phase ranging from -100" to -190". The α-phase peaks seat near of the one of substrate and the crystallographic parameters vary gradually and remain similar to those of the substrate. As it is well known the corresponding waveguides exhibit very low propagation losses (<0.5 dB/cm) and the nonlinear coefficients are not or only slightly affected by the exchange process [9]. In paragraph IV, a particular attention will be paid to investigate the quality of channel waveguides fabricated at ϱ_{LB}=2.5%. For ϱ_{LB}=2.4%, the graded response corresponding to the α-phase is completed by a large plateau extending to -425" which means that another graded layer is present at the surface. It corresponds to $\varkappa_1$-phase. For ϱ_{LB}=2.3% it is possible to observe a sharp peak with its maximum at -472". This peak corresponds to the $\varkappa_2$-phase. Reducing further the LB concentration down to 2.2%, the $\varkappa_1$- phase layer is reorganized with a maximum intensity at -410" and the $\varkappa_2$-phase peak becomes very sharp and intense and seats at -488". Therefore, as expected, reducing the LB concentration results in increasing the deformation and allows $\varkappa_1$ and $\varkappa_2$ layers to appear at the surface of the crystal [23, 24]. The XRD signal does not go to zero between $\varkappa_1$ and α-phase peaks, which means that the transition between these phases is a layer where the crystallographic parameter varies gradually.

In the case of X-cut samples, Fig. 1(b), the waveguides fabricated with ϱ_{LB} ranging from 3% to 2.6 % only α-phase is identified, the maximum peak of this phase ranging from -50" to -120". Reducing further the concentration form 2.5% to 2.2% allows observing a sharp peak corresponding to the $\varkappa_1$- phase. The intensity of the $\varkappa_1$-phase peak gradually increases as the concentration of LB is reduced, and the increase of the intensity peak is accompanied by a shift of its maximum value from -650" to -679".

It is worth to note that, contrary to what is observed on the Z-cut samples, in the case of X-cut waveguides the XRD signal goes almost to zero between $\varkappa_1$ and α-phase peaks. That means there is a sudden transition between the phases through which the crystallographic parameters vary abruptly.

In the following sections, we will see that this quite remarkable difference in the rocking curves related to the crystal orientation is correlated to strong differences between the index profiles and the nonlinearity exhibited by the waveguides.

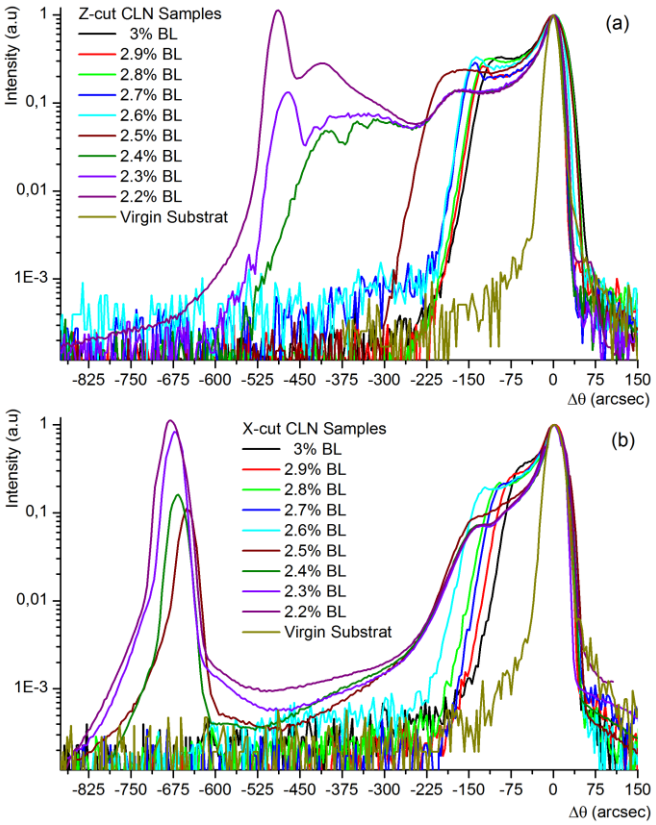

Fig. 1. (a) X-ray rocking curves from (00.12) reflection of Z-cut HiVacPE planar waveguides and (b) X-ray rocking curves from (220) reflection of X- cut HiVacPE planar waveguides. The waveguides was fabricated with different LB concentrations at T=300°C for t=72 hours.

B. Index profile reconstruction by M-lines measurements

In order to reconstruct the index profile of the planar waveguides whose crystalline structures have been presented, the effective indices of the propagation modes have been measured using a standard two-prisms coupling set-up and a He-Ne laser emitting at λ=633 nm [25].The light was in- coupled and out-coupled using rutile (TiO_2) prisms pressed against the waveguide surface. At the output of the out- coupling prism, bright lines are observed and for each one the angle with the normal to the prism output surface is measured with an autocollimator (relative error on the angle is less than 10^{-5}). This angle characterizes the propagation constant of the wave associated to the guided mode and thus we can determine the effective index of each guided mode for a given waveguide. By doing so, we identified the TM modes supported by the waveguides on Z-cut substrates and the TE modes supported by the waveguides fabricated on X-cut substrates and determined their effective index N_{eff}. From the full-set of values of N_{eff} of a given waveguide, one can reconstruct its index profile using the IWKB numerical method described in [26]. The index contrast Δn_e of a given waveguide is calculated as the difference between its surface index and the value of the extraordinary index of the substrate (n_e=2.2028 for Gooch & Housego virgin substrate). The obtained Δn_e for each LB concentration are presented on Table I. The reconstructed index profiles for Z-cut and X-cut waveguides are presented on Fig. 2.

In the case of Z-cut samples, as it can clearly be seen the HiVacPE waveguides show a gradually increase of index contrast from $\Delta n_e=1.57\times10^{-2}$ up to 1.11×10^{-1} as the LB concentration decreases in the acidic bath. As we can see in Fig. 2 (a), the index profiles change from an exponentially decreasing one to a mix of graded profiles whose shape is not precisely determined. The change from one regime to the other occurs between ϱ_{LB}=2.5% and ϱ_{LB}=2.6%, which corresponds to the ϱ_{LB} values at which the ϰ phases start to appear in the rocking curves.

It is important to note that for the same acidity of the bath, the index profile of the Z-cut HiVacPE waveguides are different from that obtained in containers where the initial pressure is approximately 1 mbar. We attribute this, to the high vacuum in the glass tube at the beginning of the HiVacPE process, which is the sign that most of the water traces have been removed. This was not the case in the melts used to prepare HISoPE waveguides [14].

TABLE I
INDEX CONTRAST AT λ=633 nm OF THE WAVEGUIDES FABRICATED BY HIVACPE ON Z-CUT AND X-CUT LN AT T=300°C FOR t=72 HOURS

	Index Contrast Δn_e	
ρ_{LB}	**Z-cut**	**X-cut**
3%	1.57×10^{-2}	1.37×10^{-2}
2.9%	1.89×10^{-2}	1.59×10^{-2}
2.8%	1.96×10^{-2}	1.94×10^{-2}
2.7%	2.25×10^{-2}	1.97×10^{-2}
2.6%	2.34×10^{-2}	3.08×10^{-2}
2.5%	3.92×10^{-2}	1.23×10^{-1}
2.4%	8.84×10^{-2}	9.53×10^{-2}
2.3%	1.02×10^{-1}	9.58×10^{-2}
2.2%	1.11×10^{-1}	9.58×10^{-2}

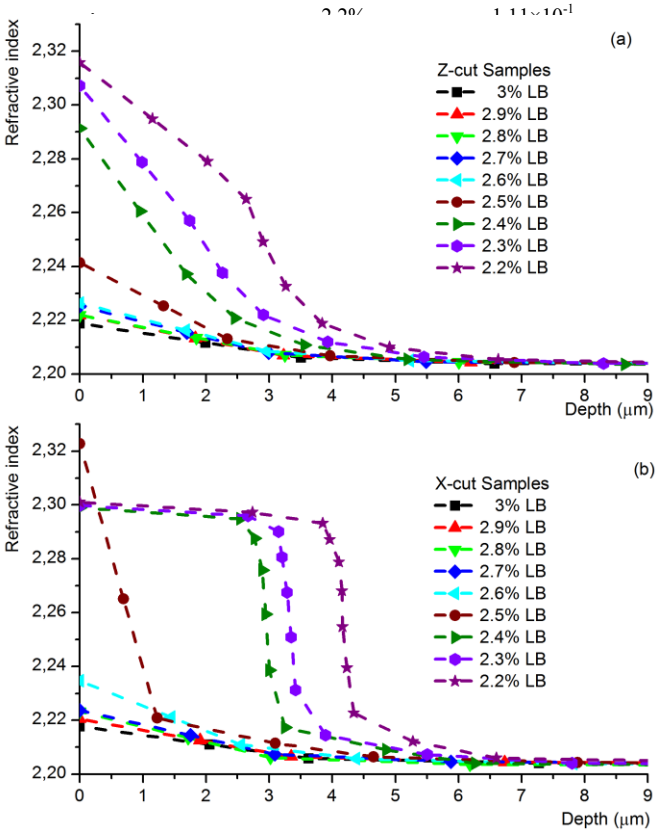

Fig. 2. Extraordinary index profile at λ=633 nm reconstructed by IWKB for planar waveguides fabricated in (a) Z-cut and (b) X-cut LN by HiVacPE using different concentration of the LB in the bath at 300°C and for 72 hours. The symbols represent the measured N_{eff} of the modes. In origin is the surface index calculated by IWKB. Dashed lines are guides for the eye.

In the case of X-cut samples, the index contrast gradually increases from Δne=1.37×10-2 up to 3.08×10-2 as ϱLB decreases from 3% to 2.6%. (see Table I). At ϱLB=2.5% an abrupt jump is observed for the surface index contrast up to Δne=1.23×10-1. This value of index contrast should be carefully considered because the IWKB method is inaccurate when an abrupt index change occurs in less than an optical wavelength, which is the case at this concentration. As we can clearly see in Fig. 2 (b), this concentration value seems to be the threshold from which the index profile exhibit a step part which can be observed down to ϱLB=2.2%.
The step index part of the index profile is not observed on Z-cut samples and this difference corresponds to the difference observed in the rocking curves. On Z-cut samples the rocking curves show different phases but in-between these phases, the signal never goes to zero, which indicate a superposition of layers were the crystallographic parameter is varying gradually just as the refractive index. On X-cut samples at the contrary, the rocking curves show a clear gap between the α and the ϰ phases, which correspond to the abrupt variation of the refractive index between the two phases.

C. Analysis of index contrast

In this next section, we thoroughly investigate the threshold ϱ_{LB} values where changes are occurring in the index profile of Z-cut and X-cut waveguides. In Fig. 3 are represented for both Z-cut and X-cut waveguides, the index contrast Δn_e vs the concentration of the LB in the acidic bath.

The idea is to identify the LB concentration threshold ρ_{th} from which one passes from a simple exponential profile to complex gradient one for Z-cut waveguides and to the mix of a step and gradient profile for X-cut waveguides. To achieve this we used several methods. First was the fit of experimental points with a sigmoidal type function such as Boltzmann $\Delta n(\varrho_{LB})=\Delta n_{e,max}/(1+\exp((\varrho_{LB}-\varrho_{th})/\tau))$ were τ is a parameter which characterizes the steepness of the curve. Using this method the fit is good but not the best and for this reason, it is not presented in Fig. 3. Other method is the fitting of the experimental points by chunks. The first chunk is fitting with a step-like modified version of Michaelis-Menten function $\Delta n(\varrho_{LB})=\Delta n_{e,max}\times(\varrho_{th}-\varrho_{LB})/(\tau+\varrho_{th}-\varrho_{LB})$ which present a discontinuity in ϱ_{th}. The second chunk is fitting with a linear regression. The intersection of these two fits gives the threshold value ϱ_{th}. This approach looks more natural and, indeed, the fits are better. However, the best fit is obtained when a sum of two generalized exponential functions are used. It is expressed by:

$$n_e(\varrho_{LB}) = n_e + A_1 \exp\left(-(\varrho_{LB}/w_i)^{a_1}\right) + A_2 \exp\left(-(\varrho_{LB}/w_2)^{a_2}\right) \qquad (2)$$

A_1, A_2, w_1, w_2, a_1 and a_2 are adjustable parameters. When the parameters $a_i=1$ the function is an exponential decay, when $a_i=2$ the function is a Gaussian and when $a_i \geq 10$ the function is a quasi-step. Each of the generalized exponential function fits one chunk of the experimental points.

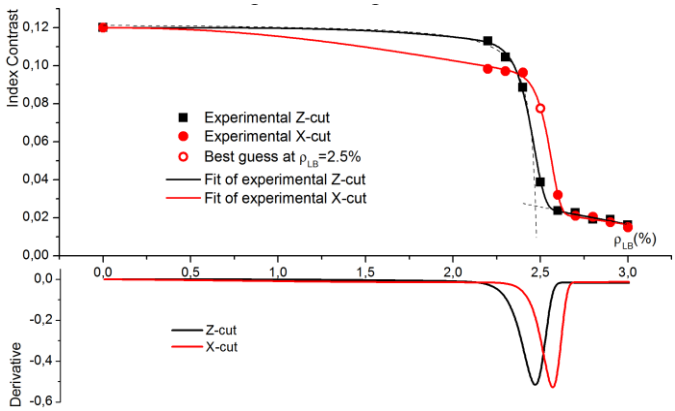

Fig. 3. Variation of the index contrast Δn_e vs LB concentration for Z-cut and X-cut waveguides. The symbols represent the experimental points and solid lines are the fits with sum of two generalized exponential functions. The dashed lines are partial fits, i.e. modified Michaelis-Menten function and linear regression. The best guess of the index contrast for X-cut sample fabricated at 2.5% is represented by a circle. On bottom part of the graph are given the derivative of the fits, which help to localize the position of the threshold after which the waveguides present only the α-phase (SPE type waveguides).

The threshold of LB concentration is obtained with very good precision when we make the derivative of the fitting curves. For each point, its derivative is calculated as the average of the left and the right derivatives. The experimental points are fitted considering the maximum index contrast at $\Delta n_{e,max}=0.12$ for both Z-cut and X-cut respectively [27]. From the full set of points corresponding of X-cut samples, the value of index contrast $\Delta n_e=1.23\times10^{-1}$ obtained for 2.5% is not used when fitting the points for the reason given above about inaccurate values given by IWKB. After appropriate fit of remained points we find for 2.5% on the fit curve the best guess of index contrast at $\Delta n_e= 7.7\times10^{-2}$. This value will be used for all other investigations and analysis in our paper.

To obtain ϱ_{th}, we calculate the minimum of the derivatives of the index contrast vs ϱ_{LB} curves which gives: $\varrho_{th,Z-cut}=2.46\pm0.03\%$ for Z-cut waveguides and $\varrho_{th,X-cut}=2.53\pm0.03\%$ for X-cut waveguides. These points give the threshold after which the index profiles of the waveguides are no longer a simple exponential profiles. This threshold corresponds exactly to the one that can be defined looking at the appearance of $\varkappa$ phases in the rocking curves.

D. Analysis of index profiles

In this section, we thoroughly analyze the index profiles in order to determine the best fit for the experimental points depicted in Fig. 2. We will use, once again, the sum of two generalized exponential functions expressed by:

$$n(d) = n_e + A_1 \exp\left(-(d/w_i)^{a_1}\right) + A_2 \exp\left(-(d/w_2)^{a_2}\right) \qquad (2)$$

where, once again, A_1, A_2, w_1, w_2, a_1 and a_2 are adjustable parameters and take different values depending on LB concentration and d is the depth in the waveguide. Each generalized exponential function in (3) describes the behavior of one of the chunk of the index profile. Therefore, for waveguides exhibiting only a simple exponential profile the second function in (3) vanishes.

On Fig. 4 are plotted index profiles for the Z-cut samples fabricated with ϱ_{LB} equal to 2.2%, 2.3% and 2.4%, which are the only ones exhibiting complex profiles. The symbols represent de measured N_{eff} of the propagating modes and at the origin is the surface index calculated by IWKB. The solid lines are the fits obtained by using (3) and dashed lines are partial fits using modified Michaelis-Menten function and exponential decay. The derivatives of the fits exhibit one minimum point for 2.4% and two minimum points for both 2.2% and 2.3% respectively. These minimum points correspond to a given depth in the waveguide, where there is a significant refractive index difference between two layers. The derivative curve corresponding to 2.4% exhibits only one minimum point, which means that this waveguide exhibits two refractive index sub-layers. First sub-layer starts from the surface of the waveguide and extends until approximately 1 µm in depth and then starts the second sub-layer which goes to the end of the protonated area (see inset on Fig 4 for two sub- layers configuration of the waveguide). Further, for both 2.2% and 2.3% respectively the derivative curves exhibit two minimum points, which means that these waveguides exhibit three refractive index sub-layers (see inset on Fig 4 for three sub-layers configuration of the waveguide).

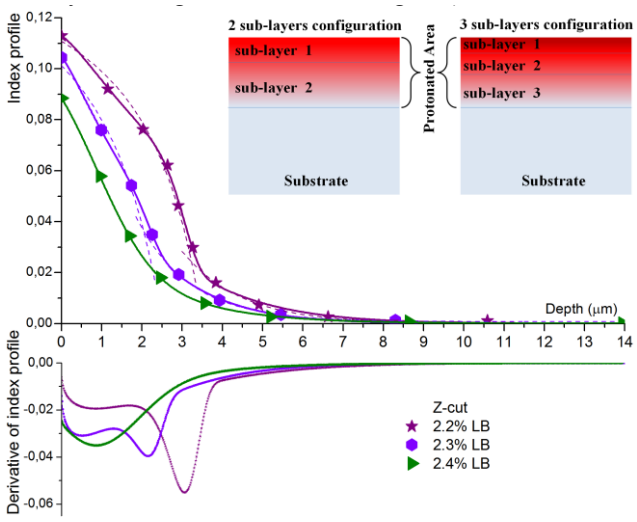

Fig. 4. Index profiles of Z-cut HiVacPE waveguides fabricated with LB concentration ranging from 2.2% to 2.4% respectively. The symbols represent de measured Neff of the propagating modes and at the origin is the surface index calculated by IWKB. The solid lines are the fits obtained by using (3) and dashed lines are partial fits using modified Michaelis-Menten function and exponential decay. In the bottom part of the graph are given the derivative of the fits. In the inset are represented the sub-layers structures of the waveguides. The intensity of the red color represents the refractive index value in the waveguides.

In this case, first sub-layers start from the surface and extends until approximately 0.5 µm and 0.8 µm in depth for 2.3% and 2.2% respectively. From these depths start the second sub- layers that go to 2.2 µm and 3 µm for 2.3% and 2.2% respectively. Then, the third sub-layers start and go dipper to the end of the protonated areas. These results are consistent with what has been observed on the rocking curves with the apparition of a $\varkappa_1$ layer and later a $\varkappa_2$ layer when ϱ_{LB} is reduced from 2.4% to 2.2%.

On Fig. 5 are plotted the index profiles for the X-cut samples fabricated with LB concentrations ranging from 2.2% to 2.5%. The symbols represent de measured N_{eff} of the propagating modes and at the origin is the surface index calculated by IWKB or the best guess value for $?_{LB}$=2.5%. The solid lines are the fits obtained by using (3) and dashed lines are partial fits using modified Michaelis-Menten function and exponential decay. The derivative curves exhibit only one minimum point for any of these profiles. These minimum points correspond to a given depth in the waveguide, where there is a significant refractive index difference between two layers. For ϱ_{LB}=2.5%, the first sub-layer starts from the surface of the waveguide and extends to approximately 0.9 µm As expected, by decreasing ϱ_{LB}, the first sub-layer goes dipper to approximately 3 µm, 3.5 µm and 4.5 µm for ϱ_{LB}=2.4%, ϱ_{LB}=2.3% and ϱ_{LB}=2.2% respectively. From these points start the second sub-layers, which go to the end of the protonated area. See the inset of Fig. 5 for both: two sub-layers configuration of the waveguide and relationship between the thickness of the first sub-layer and LB concentration. Once again, these results can be directly correlated with the rocking curves where only the $\varkappa_1$ phase has been identified for the low values of ϱ_{LB} used in this study.

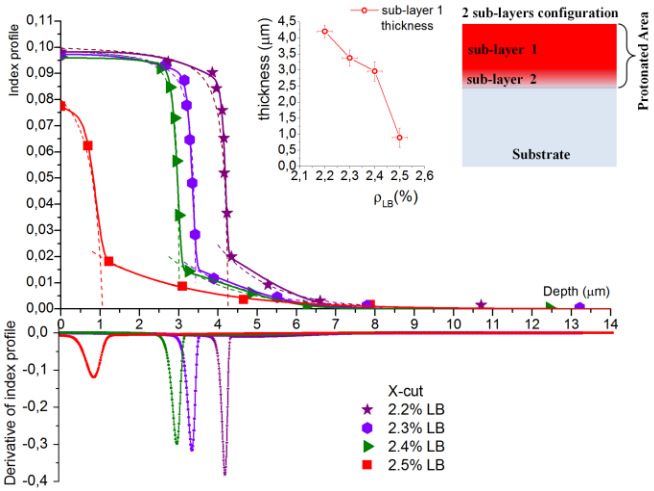

Fig. 5. Index profiles of X-cut HiVacPE waveguides fabricated with LB concentrations ranging from 2.2% to 2.5% respectively. The symbols represent de measured Neff of the propagating modes and at the origin is the surface index calculated by IWKB or the best guess value for 2.5%. The solid lines are the fits obtained by using (3) and dashed lines are partial fits using modified Michaelis-Menten function and exponential decay. On the bottom part of the graph are given the derivative of the fits. In the inset are represented the sub-layers structures of the waveguides. The intensity of the red color represents the refractive index value in the waveguides.

E. Nonlinearity Measurements

One of the great interests of LN waveguides is their high nonlinear efficiency. In order to see if the HiVacPE technique preserves the nonlinearity of the material, we performed surface Second Harmonic Generation (SHG) measurements. The experimental setup is similar to the one used in [13] and which is fully described in [28]. A laser beam at wavelength 1.5 µm is focused on the polished end facet of a waveguide and vertically scanned through the different regions: air, exchanged layers and substrate respectively. By measuring, during the scan, the reflected fundamental and second harmonic (SHG) beams, one can evaluate the variation of the second–order nonlinearity coefficient induced by the waveguide fabrication process. The fundamental beam is used to identify the air-waveguide interface position and the intensity of the harmonic is used to compare the waveguide value of the nonlinear coefficient d_{33} with its substrate value.

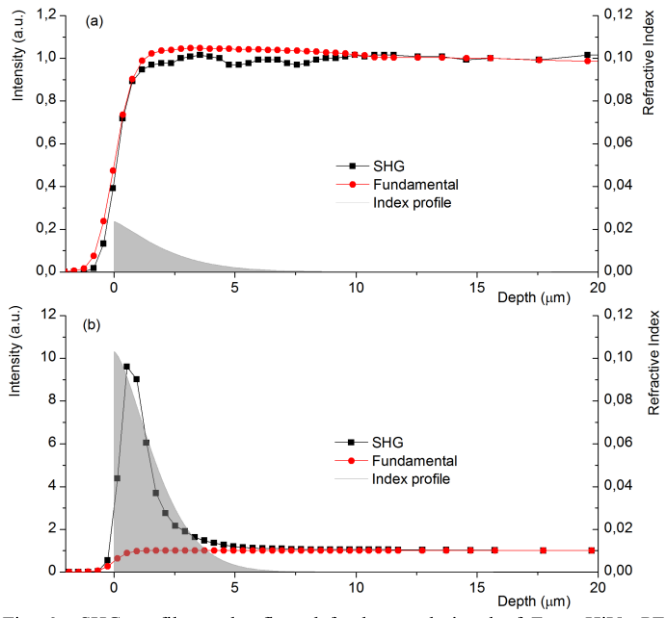

Fig. 6. SHG profiles and reflected fundamental signal of Z-cut HiVacPE waveguides superimposed with index profiles when (a) ϱ_{LB} decreases from 3% to 2.5% and (b) ϱ_{LB} decreases from 2.4% to 2.2%.

In Fig. 6 (a) is presented a typical example of these scan superimposed with the corresponding index profile at λ=633 nm for a Z-cut waveguide fabricated with ϱ_{LB} ranging from 3% to 2.5%. These waveguides exhibit only one single layer and no ϰ phase. As it can be seen, there is no significant variation of SHG signal between the protonated area and the substrate. This indicates that the waveguides exhibit the same nonlinear coefficient as the substrate when only α-phase is present in the proton exchanged layer. This result is identical to the one obtained in all the waveguides produced so far and presenting only the α-phase in the protonated area. Reducing further ϱ_{LB} from 2.4% to 2.2%, the waveguides exhibit, as we have already seen, either two or three sub-layers. In these cases, the SHG and fundamental signals are similar to the ones presented on Fig 6 (b). Besides the α-phase, these waveguides contain ϰ phases and exhibit a very high index

contrast in a part of the waveguide. For these waveguides, the SHG peak is very sharp and intense compared the other ones. The SHG signal superimposed on the refractive index profile of the waveguide clearly shows an intense peak of SHG in the protonated area. This enhancement of the SHG signal is probably a complex function of the discontinuity of the nonlinear coefficient d_{33} between the air and the crystal [29] and of the confinement of the pump beam due to the high index contrast in the waveguide. Therefore, without a complete understanding of the reflected SHG signal, it is impossible to extract information about the exact value of the nonlinear coefficient d_{33} in these HiVacPE waveguides, but we can assume at least that the waveguide value is equal to the substrate value.

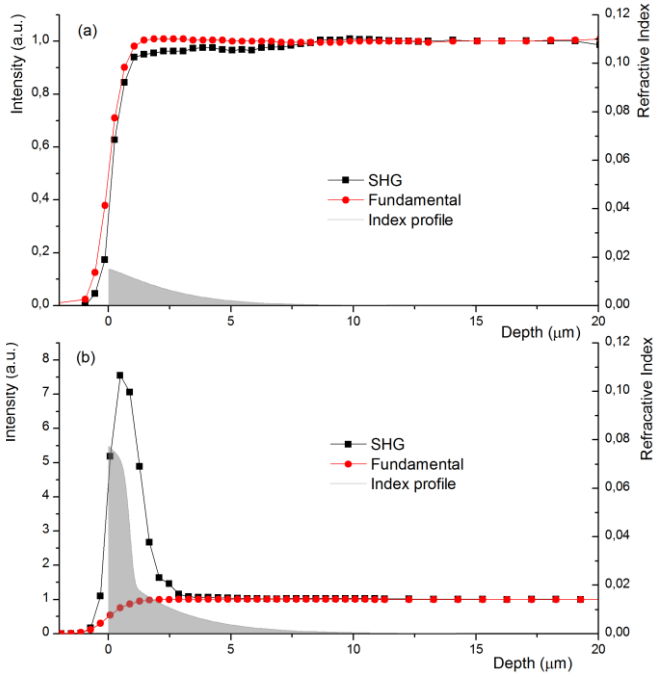

Fig. 7. SHG profiles and reflected fundamental signal of X-cut HiVacPE waveguides superimposed with index profiles when (a) ϱLB decreases from 3% to 2.6% and (b) ϱLB=2.5%

In Fig. 7 (a) is presented one example of the SHG and fundamental signal for X-cut waveguides superimposed with the index profile at λ=633 nm of the waveguide when ϱ_{LB} decreases from 3% to 2.6%. These waveguides exhibit one single layer and a low index contrast. As it can be seen, there is no significant variation of the SHG signal between the protonated area and the substrate. This indicates that the waveguides exhibit the same nonlinear coefficient as the substrate when only α-phase is presented in the protonated area, as already observed in waveguides fabricated in other experimental conditions. On Fig. 7 (b) is presented the very sharp and intense SHG peak exhibited by the waveguide fabricated at ϱ_{LB}=2.5%. Besides the α-phase, this waveguide contains $\varkappa_1$-phase and exhibit a high index contrast. The intense peak of SHG that is observed here has probably the same origin as the one observed on Z-cut samples. Moreover, due to the lateral resolution of the experiment (~2μm) and the small depth of the $\varkappa$ layer (0.9μm) it is impossible to extract a clear information about the value of d_{33} in the surface layer of this particular waveguide.

Now, it is worth presenting in Fig. 8 each SHG and fundamental signal obtained on samples prepared with a LB concentration ranging from 2.4% to 2.2%. These waveguides exhibit two sub-layers and an index profile composed of a step part and a graded part. The first important thing to note is that the nonlinearity is not preserved in more than half of the first index sub-layers of the protonated area. It is difficult to be more precise concerning the exact extension of the area where d_{33} is reduced, due to the lateral resolution of the experiment and of the presence of the SHG peak which, in this case, tends to exists at the interface between the $\varkappa$ and the α layers. When looking more closely, the second thing to note is that the nonlinearity is not completely destroyed at the surface of the waveguides for the concentrations 2.4% and 2.3% (see Fig. 8 (a) and (b)). At the contrary, for 2.2%, the SHG signal remains equal to zero starting from the surface down to almost 2.5 μm (see Fig. 8 (c)).

This quite remarkable different behavior of the nonlinearity depending on the substrate orientation is in very good agreement with the index profiles and with the XRD analysis. In the case of Z-cut waveguides, the XRD signal does not go to zero between the different phases. The transition between these phases is done

through a layer in which the crystallographic parameter varies gradually, which is also observed in the index profile and allows observing high index layers with no degradation of the nonlinear coefficient d_{33}. At the contrary, for the X-cut waveguides the XRD signal goes almost to zero between $\varkappa_1$ and α phases, and the crystallographic parameter varies abruptly between them. This induces a sudden strain transition that can be also observed in the index profile of the waveguides and is correlated with a strong degradation of the nonlinearity.

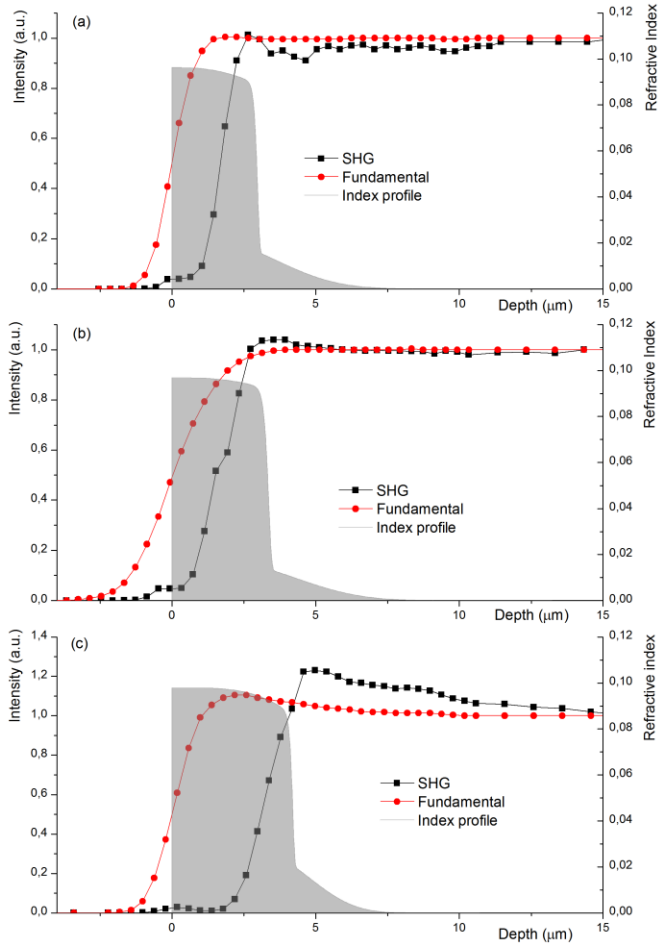

Fig. 8. SHG profiles and reflected fundamental signal of X-cut HiVacPE waveguides superimposed with index profiles when (a) ϱ_{LB}=2.4%, (b) ϱ_{LB}=2.3% and (c) ϱ_{LB}=2.2%.

IV. HiVacPE CHANNEL WAVEGUIDES

A. Fabrication of channel waveguide

In view of the possible applications, we have targeted the fabrication of single-mode channel waveguides around λ=1550 nm. Taking into account that, decreasing the LB concentration in the melt increases the index contrast Δn_e, we have to adjust the width of the waveguide so that it remains single-mode at the wavelength of interest. Therefore, channel waveguides were fabricated by using SiO_2 masks with openings of different width. They were fabricated on the surface of Z-cut samples using standard UV photolithography, Ion Assisted Deposition (IAD) of SiO_2 layer and a lift-off process. Besides a set of channel waveguides, the so prepared samples have the advantage to present on the opposite surface, a planar waveguide very useful for preliminary M-lines characterizations. It is worth to note that depending on the openings in the SiO_2 mask, some of the channel waveguides exhibit smaller depths than the planar waveguide, due to the fact that, through narrow opening, the lateral diffusion is no longer negligible [30]. To allow characterizing the channel waveguides, the input and the output edges of the samples were polished with high quality.

B. Propagation losses

Propagation losses in the HiVacPE channel waveguides have been measured by using the Fabry-Pérot cavity technique [31]. For each channel waveguide, the single mode propagation was tested by investigating the

near-field pattern at the output of the waveguide. The high quality of the edges polishing makes the investigated waveguide to act as a resonant optical cavity. Resonance conditions depend on the wavelength so their periodic occurrence can be evidenced by varying the wavelength of a tunable laser around λ=1550 nm and measuring the transmitted intensity. The propagation losses P (evaluated in decibels) can be retrieved from the oscillation contrast using:

$$P = 4.34\left[\ln(R) - \ln\frac{1-(1-C^2)^{1/2}}{C}\right] \qquad (4)$$

were R is the end-face (Fresnel) reflection coefficient taking in account the mode waists and the angles formed by the waveguide with the end faces of the sample. The parameter C is the contrast defined as:

$$C = \frac{I_{max} - I_{min}}{I_{max} + I_{min}}$$

were I_{max} and I_{min} represent the maximum and minimum output intensities, respectively.
The modal behavior was verified by observing the near- field pattern of the propagating mode for each channel waveguide. The investigations were performed by using a tunable laser (Yenista Optics – Tunics T100R) around λ=1550 nm. For the in-coupling we used a micro lensed polarization maintaining fiber. The image of the propagating modes at the waveguide output is obtained with an Olympus microscope objective and an infrared highly sensitive CCD camera (NIR- 300PGE from VDS Vosskühler GmbH). The investigation results on propagation losses can be grouped into two categories as follow:

1. Propagation losses for low-index contrast
For the ϱ_{LB} ranging from 3% to 2.5%, corresponding to low index contrast, we experimentally validate the single-mode behavior at λ=1550 nm. In the case of channel waveguides fabricated using 2.5% of LB and 6μm opening, the oscillation contrast (C=20±2%) can be deduced from the spectra depicted in Fig. 9. It should be noted the fact that the index contrast for 2.5% is the highest index contrast value for what is generally called the range of low-index contrast waveguides. The best of our investigated channel waveguides exhibit very low propagation losses around 0.16±0.02 dB/cm.

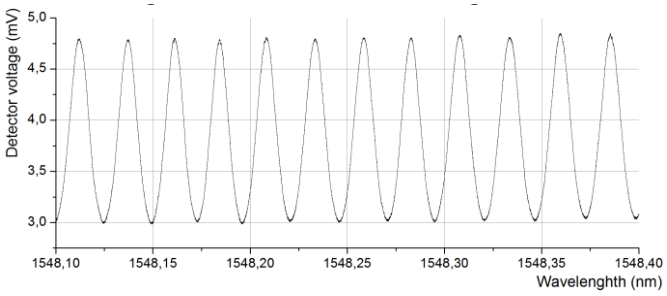

Fig. 9. Transmission of a Fabry-Pérot waveguide cavity fabricated by using 2.5% of LB and opening of 6μm on the mask.

2. Propagation losses for high-index contrast
For the lower LB concentrations ranging from 2.4%, to 2.2%, allowing to get very high index contrast, the channel waveguides were fabricated by using openings in the mask of width 2 μm and 2.5 μm, in order to obtain single-mode propagation at λ=1550 nm.
In Fig. 10 (a) and (b) we present the near-field pattern of the optical modes supported by a channel waveguide prepared with ϱ_{LB}=2.2% and 2 μm opening. Unfortunately, we can clearly observe a multimode behavior at λ=1550 nm. Furthermore, we observe, a certain amount of radiating light around the propagating mode. This makes us thinking of TM- TE polarization coupling which would lead to the arising of hybrid modes (EH modes) [32, 33]. To verify this aspect we observed the far field at the output of the waveguide by using a visible light at λ=633 nm. In order to separate TM and TE polarizations, a polarizer was introduced between the sample and the screen placed just a few centimeters away. When only TE polarization is passing, it can be observed characteristic semicircles corresponding to the light radiating into the substrate, the

waveguide acting like an antenna. A part of radiating light is reflected by the bottom surface of the sample, resulting in mirrored semicircles in the upper half of the image on Fig. 10 (c).

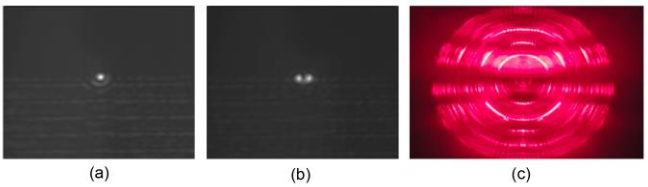

Fig. 10. Near field pattern (a) and (b) of optical modes supported by a channel waveguide prepared with ϱ=2.2% and 2µm width. (c) Far field picture on a screen of TE polarized hybrid modes in HiVacPE channel waveguide at λ=633 nm

The hybrid modes were already observed in proton exchanged Z-cut LN waveguides and the hybrid nature of the modes was clearly related to the index modifications due to the important strain that can be induced by the proton exchange process in certain fabrication conditions [14, 32, 33]. Unfortunately, the multimode behavior of the propagation makes no longer possible to use the Fabry-Pérot cavity technique. Despite the fact that the planar waveguides on the opposite face of the sample exhibited quite good optical quality during M-lines measurements, even for the low concentrations of the BL ranging from 2.4% to 2.2%, we assume high losses (? 5 dB/cm) for the channel waveguides fabricated in these conditions. These are mainly due to the strain induced by non- modified area of the crystal all around the waveguide [14]. The strain induced index modifications cause TM-TE polarization coupling which leads to the arising of hybrid modes (EH modes) whose ordinary part can radiate in the substrate.

V. DISCUSSION AND CONCLUSION

In this paper, we describe a new waveguide fabrication technique in LN that we named High Vacuum Proton Exchange (HiVacPE). If the main purpose was to improve the reproducibility and the quality of the produced waveguides by limiting and controlling the water traces in the melt, we discovered that, when the acidity of the bath is increased, depending on substrate orientation (Z-cut or X-cut) the waveguides are completely different in term of crystallographic properties, index profiles and nonlinearity. By comparing the HiVacPE waveguides to the waveguides fabricated by any other PE process we shown that the high vacuum modifies the results and shifts certain important characteristics such as the position of ϱ_{th} thresholds.

For $\varrho_{LB} > \varrho_{th}$ the exchanged layer is in α-phase and the properties of the waveguides are those of the well-known SPE waveguides: low index contrast, exponential index profiles and preserved nonlinearity. For the channel waveguides fabricated in these conditions, propagation losses around 0.16dB/cm are experimentally validated. As we already said, these waveguides are quite similar to SPE waveguides, but one has to note that HiVacPE process allows fabricating waveguides with an index contrast up to 0.04 which is the highest index contrast ever reported in the literature for such lithium niobate channel waveguides. Most probably, these waveguide fabrication conditions are compatible with periodically poled substrates, and therefore should allow fabricating very efficient nonlinear components for quantum or classical optical data processing.

However, for ϱ_{LB} slightly lower to ϱ_{th}, our characterizations point out a phenomenon that has never been reported so far. Waveguides produced with such melts present completely different characteristics depending on the fact that the sample is Z-cut or X-cut.

From XRD analysis, we clearly observe that the crystallographic structures of HiVacPE waveguides are completely different depending on substrate orientation (Z-cut or X-cut), The Z-cut samples present several layers where the crystallographic parameter varies gradually with smaller jump between the phases while the X-cut samples exhibit an abrupt transition between the α and the $\varkappa_1$ phases.

A clear difference is also visible when working on the index profiles of the produced waveguides, the Z-cut and the X-cut samples exhibiting completely different shapes. The Z-cut waveguides exhibit complex gradient index profiles, while the X-cut waveguides exhibit a first layer where the index is constant followed by a second layer where it is exponentially varying down to the substrate value. We demonstrated that these index profiles of the waveguides fit very well with the sum of two generalized exponential functions. The careful analysis of these fits, revealed the layered structure of the waveguides.

The measurement of the local nonlinearity, also indicate a strong difference when fabricating HiVacPE waveguides with $\varrho_{LB} < \varrho_{th}$ on Z-cut and X-cut samples. In the high index part of the waveguides, the nonlinearity is mostly preserved for the Z- cut samples, while on the X-cut ones it is drastically reduced or destroyed depending on the ϱ_{LB} value. This indicates that, by using HiVacPE process the high-index contrast nonlinear
waveguides can only be obtained on Z-cut substrates although nothing has suggested this aspect if we consider the results presented in [34]. At the contrary, the high propagation losses of channel waveguides presenting a high index increase, is not a surprise. They are due to stress induced index modification resulting in TE-TM coupling, which in a material where the birefringence is negative and where only the extraordinary modes (TM modes in this case) are guided results in losses through the radiation into the substrate of the ordinary component of the modes.
In order to use the highest index contrasts obtained by HiVacPE, there is still some work to do, such as fabricating a planar HiVacPE waveguide and then etch most of the surface of the sample to define ridge waveguides. In this case, the waveguides will not be laterally stressed and therefore one can avoid TE-TM conversion that induces most of the high propagation losses observed in the channel waveguides fabricated up to now.
In summary, we have demonstrated that pumping harder the exchange ampoule to diminish as much as possible the water content in the acidic bath used to fabricate waveguides in LN, resulted in a new proton exchange technique the so-called High Vacuum Proton Exchange (HiVacPE).
Taking advantage of simultaneously exhibited index contrast as high as 0.04, low propagation losses (0.16dB/cm) and preserved nonlinearity, the HiVacPE technique can be a way of improving the efficiency of the nonlinear components and devices in many applications using LN waveguides.
We have also demonstrated that the HiVacPE process allows fabricating waveguides on Z-cut LN exhibiting high- index contrast up to 0.11 without degrading the crystal nonlinearity, which combined with an appropriate etching process, allows fabricating nonlinear photonic wires. This is of high interest for nonlinear highly efficient and compact devices for quantum and classical optical data processing.
The impact on the reproducibility was tested by producing in same conditions more than fifty waveguides during one year and a half and no notable differences were identified.
In addition to the difference of our waveguides compared to ones fabricated by any other proton exchange process, the quite remarkable aspect that stands out is the fact that, depending on substrate orientation the waveguides exhibit completely different crystallographic structures, index profile shapes and nonlinear properties.
Moreover, we proposed an original and very useful method of analyzing waveguides exhibiting complex index profiles. This method can be used for the analysis of the waveguides fabricated by any other proton exchange techniques.

REFERENCES

[1] W. Sohler, H. Hu, R. Ricken, V. Quiring, C. Vannahme, H. Herrmann, D. Büchter, S. Reza, W. Grundkötter, S. Orlov, H. Suche, R. Nouroozi, and Y. Min, "Integrated Optical Devices in Lithium Niobate," Opt. Photon. News, vol. 19, no. 1, pp. 24-31, Jan. 2008.
[2] G. Schreiber, D. Hofmann, W. Grundkoetter, Y. L. Lee, H. Suche, V. Quiring, R. Ricken, and W. Sohler, "Nonlinear integrated optical frequency converters with periodically poled Ti:$LiNbO_3$ waveguides," in Proc. SPIE, Integrated Optics Devices V, vol. 4277, pp. 144-160, May 15, 2001.
[3] M. H. Chou, I. Brener, G. Lenz, R. Scotti, E. E. Chaban, J. Shmulovich, and M. M. Fejer, "Efficient wide-band and tunable midspan spectral inverter using cascaded nonlinearities in $LiNbO_3$ waveguide," IEEE Photon. Technol. Lett., vol. 12, no. 1, pp. 82-84, Jan. 2000.
[4] M. Asobe, O. Tadanaga, H. Miyazawa, Y. Nishida, and H. Suzuki, "Multiple quasi-phase-matched device using continuous phase modulation of $\chi^{(2)}$ grating and its application to variable wavelength conversion," IEEE J. Quantum Electron., vol. 41, no. 12, pp. 1540-1547, Dec. 2005.
[5] I. Brener, B. Mikkelsen, G. Raybon, R. Harel, K. Parameswaran, J. R. Kurz, and M. M. Fejer, "160 Gbit/s wavelength shifting and phase conjugation using periodically poled $LiNbO_3$ waveguide parametric converter," Electron Lett., vol. 36, no. 21, pp. 1788-1790, Oct. 2000.

[6] K. Parameswaran, R. Route, J. Kurz, R. Roussev, M. Fejer, and M. Fujimura, "Highly efficient second-harmonic generation in buried waveguides formed by annealed and reverse proton exchange in periodically poled lithium niobate," Opt. Lett., vol. 27, no. 3, pp. 179-181, Feb. 2002.
[7] L. Chanvillard, P. Aschieri, P. Baldi, D. B. Ostrowsky, M. De Micheli, L. Huang, and D. J. Bamford, "Soft proton exchange on PPLN: A simple waveguide fabrication process for highly efficient non-linear interactions," Appl. Phys. Lett., vol. 76, no. 9, pp. 1089–1091, Feb. 2000.
[8] Y. N. Korkishko, V. A. Fedorov, E. A. Baranov, M. V.Proyaeva, T. V. Morozova, F. Caccavale, F. Segato, C. Sada, an S. M. Kostritskii, "Characterization of alpha-phase soft proton-exchanged $LiNbO_3$ optical waveguides," J. Opt. Soc. Amer. A, vol. 18, no. 5, pp. 1186–1191, May 2001
[9] D. Castaldini, P. Bassi, P. Aschieri, S. Tascu, M. De Micheli, and P. Baldi "High performance mode adapters based on segmented SPE:$LiNbO_3$ waveguides," Opt. Express, vol. 17, no. 20, pp. 17868-17873, Sep. 2009.
[10] D. Castaldini, P. Bassi, S. Tascu, P. Aschieri, M. De Micheli, and P. Baldi "Soft Proton Exchange tapers for low insertion loss LiNbO3 devices," J. Lightwave Technol., vol. 25, no. 6, pp. 1588-1593, June 2007.
[11] F. Caccavale, P. Chakraborty, A. Quaranta, I. Mansour, G. Gianello, S. Bosso, R. Corsini, and G. Mussi, "Secondary-ion-mass spectrometry and near-field studies of Ti:$LiNbO_3$ optical waveguides," J. of Appl. Phys., vol. 78, no. 9, pp. 5345-5350, Nov. 1995.
[12] J. L. Jackel, C. E. Rice, and J. J. Veselka, "Proton exchange for high-index waveguides in $LiNbO_3$," Appl. Phys. Lett., vol. 41, no. 7, pp. 607- 608, Oct. 1982.
[13] F. Laurell, M. G. Roelofs, and H. Hsiung, "Loss of optical nonlinearity in proton-exchanged $LiNbO_3$ waveguides," Appl. Phys. Lett., vol. 60, no. 3, pp. 301–303, Jan. 1992.
[14] O. Stepanenko, E. Quillier, H. Tronche, P. Baldi, and M. De Micheli "Crystallographic and Optical Properties of Z-Cut High Index Soft Proton Exchange (HISoPE) $LiNbO_3$ Waveguides," J. Lightwave Technol., vol. 34, no. 9, pp. 2206-2212, May 2016.
[15] A. Loni, R. M. De La Rue, and J. M. Winfield "Proton exchanged, lithium niobate planar-optical waveguides: Chemical and optical properties and room-temperature hydrogen isotopic exchange reactions," J. Appl. Phys., vol. 61, no. 1, pp. 64-67, Jan. 1987.
[16] Y. S. Son, H. J. Lee, Y. K. Jhee, S. Y. Shin, and B. G. Kim "Fabrication of $LiNbO_3$ channel waveguides using water," IEEE Photon. Tech. Lett., vol. 4, no. 5, pp. 457-459, May 1992.
[17] J. Rams, and J. M. Cabrera "Characterization of $LiNbO_3$ waveguides fabricated by proton exchange in water," Appl. Phys. A, vol. 81, no. 1, pp. 205–208, June 2005.
[18] Y. S. Son, H. J. Lee, Y. K. Jhee, S. Y. Shin, and B. G. Kim " Fabrication of $LiNbO_3$ channel waveguides using water," IEEE Photon. Tech. Lett. vol. 4, no. 5, pp 457-459, May 1992.
[19] W. L. Marshall, and E. U. Franck "Ion Product of Water Substance, 0- 1000°C, 1-10,000 Bars. New International Formulation and Its Background," J. Phys. Chem. Ref. Data, vol.10, no.2, pp. 295-304, Apr. 1981.
[20] S. S. Mushinsky, A. M. Minkin, I. V. Petukhov, V. I. Kichigin, D. I. Shevtsov, L. N. Malinina, A. B. Volyntsev, M. M. Neradovskiy, and V. YA. Shur "Water Effect on Proton Exchange of X-cut Lithium Niobate in the Melt of Benzoic Acid," Ferroelectrics, vol. 476, no. 1, pp. 84–93, Mar. 2015.
[21] O. Stepanenko, E. Quillier, H. Tronche, P. Baldi, and M. De Micheli "Highly confining proton exchanged waveguides on Z-cut LiNbO3 with preserved nonlinear coefficient," IEEE Photon. Technol. Lett., vol. 26, no. 15, pp. 1557-1560, Aug. 2014.
[22] C. E. Rice "The structure and properties of $Li_{1-x}H_xNbO_3$," J. Solid State Chem., vol. 64, no. 2, pp. 188-199, Sept. 1986.
[23] Yu. N. Korkishko, and V. A. Fedorov "Structural phase diagram of $H_xLi_{1-x}NbO_3$ waveguides: The correlation between optical and structural properties," IEEE J. Sel. Top. Quantum Electron., vol. 2, no. 2, pp. 187-196, June 1996.
[24] Y. Korkishko, V. Fedorov, M. De Micheli, P. Baldi, K. El Hadi, and A. Leycuras "Relationships between structural and optical properties of proton- exchanged waveguides on Z-cut lithium niobate," Appl. Opt., vol. 35, no. 36, pp. 7056-7060, Dec. 1996.
[25] P. K. Tien, and R. Ulrich, "Theory of prism-film coupler and thin-film light guides," J. Opt. Soc. Am., vol. 60, no. 10, pp. 1325–1337, Oct. 1970.
[26] J. M. White, and P. F. Heidrich, "Optical waveguide refractive index profiles determined from measurement of mode indices: a simple analysis," Appl. Optics, vol. 15, no. 1, pp. 151-155, Jan. 1976.
[27] V. A. Ganshin and Yu. N. Korkishko "Kinetic model of proton-lithium exchange in $LiNbO_3$ and $LiTaO_3$ crystals: The role of cation vacancies," Solid State Ionics, vol. 58, no. 1-2, pp. 23-32, Nov. 1992.

[28] K. El Hadi, M. Sundheimer, P. Aschieri, P. Baldi, M. P. De Micheli, D. B. Ostrowsky, and F. Laurell, "Quasi-phase-matched parametric interactions in proton-exchanged lithium niobate waveguides," J. Opt. Soc. Am. B, vol. 14, no. 11, pp. 3197–3203, Nov. 1997.
[29]J. Kaneshiro, S. Kawado, H. Yokota, Y. Uesu, and T. Fukui "Three- dimensional observations of polar domain structures using a confocal second harmonic generation interference microscope," J Appl. Phys. vol. 104, no. 5, pp. 054112, Sept. 2008.
[30] Q. He, M.P. De Micheli, D.B. Ostrowsky, E. Lallier, J.P. Pocholle, M. Papuchon, F. Armani, D. Delacourt, C. Grezes-Besset and E. Pelletier "Self-frequency-doubled high δn proton exchanged Nd: $LiNbO_3$ waveguide laser," Opt. Commun., vol. 89, no.1, pp. 54-58, April 1992.
[31] D. Castaldini, P. Bassi, S. Tascu, G. Sauder, P. Aschieri, M. de Micheli, P. Baldi, K. Thyagarajan, and M. R. Shenoy, "All-in-one measurement setup for fast and accurate characterization of linear guided-wave optical devices," Opt. Eng., vol. 46, no. 12, pp.124601, Dec. 2007.
[32] S. Chen, P. Baldi, M. P. De Micheli, D. B. Ostrowsky, A. Leycuras, G. Tartarini, and P. Bassi "Loss mechanisms and hybrid modes in high-δne proton-exchanged planar waveguides," Opt. Lett., vol. 18, no. 16, pp. 1314- 1316, Aug. 1993.
[33] A. Knoesen, T. K. Gaylord, and M. G. Moharam "Hybrid Guided Modes in Uniaxial Dielectric Planar Waveguides," J. Lightwave Technol., vol. 6, no. 6, pp. 1083-1104, June 1988.
[34] O. Stepanenko "Towards proton exchanged quantum wires and highly confining integrated circuits on $LiNbO_3$" PhD dissertation, Nice Sophia Antipolis Univ., Nice, France, 2013.